

Soft processes at the LHC

I: Multi-component model

M.G. Ryskin^{a,b}, A.D. Martin^a and V.A. Khoze^{a,b}

^a Institute for Particle Physics Phenomenology, University of Durham, Durham, DH1 3LE

^b Petersburg Nuclear Physics Institute, Gatchina, St. Petersburg, 188300, Russia

Abstract

We emphasize the sizeable effects of absorption on high-energy ‘soft’ processes, and, hence, the necessity to include multi-Pomeron-Pomeron interactions in the usual multi-channel eikonal description. We present a model which includes a complete set of the multi-Pomeron vertices and which accounts for the diffusion in both, the impact parameter and $\ln(k_t)$, of the parton during its evolution in rapidity. We tune the model to the available data for soft processes in the CERN-ISR to Tevatron energy range. We make predictions for ‘soft’ observables at the LHC.

1 Motivation

There are three main reasons for revisiting soft pp high energy interactions at this time.

A. This paper is concerned with the description of the high energy behaviour of “soft” observables such as σ_{tot} , $d\sigma_{\text{el}}/dt$, $d\sigma_{\text{SD}}/dtdM^2$, particle multiplicities etc. in terms of basic physics. This physics predated QCD and is sometimes regarded as the Dark Age of strong interactions. However, it is unfair to call this the Dark Age. We had a successful description of these processes in terms of the exchange of Regge trajectories linked to particle states in

the crossed channels [1]. The dominant exchange at high energy is the Pomeron, and we have Gribov's Reggeon calculus [2] to account for the multi-Pomeron contributions. However the available data did not reach high enough energy to distinguish between the different scenarios [3, 4] for the high-energy behaviour of the interaction amplitude [5, 6].

In the 'weak coupling' scenario the total cross section $\sigma_{\text{tot}}(s \rightarrow \infty) \rightarrow \text{const}$, and in order not to violate unitarity, and to satisfy the inequality

$$\sigma_{\text{SD}} = \int \frac{d\sigma_{\text{SD}}}{dM^2} dM^2 < \sigma_{\text{tot}}, \quad (1)$$

the triple-Pomeron vertex must vanish when $t \rightarrow 0$, that is the triple-Pomeron coupling $g_{3P} \propto t$. In this case, the large logarithm coming from the integration over the mass of the system produced in diffractive dissociation ($\int dM^2/M^2 \simeq \ln s$) is compensated by the small value of the mean momentum transferred through the Pomeron, $\langle t \rangle \propto 1/\ln s$.

On the other hand, in the 'strong coupling' scenario, where $\sigma_{\text{tot}} \propto (\ln s)^\eta$ with $0 < \eta \leq 2$, the inequality (1) is provided by a small value of the rapidity gap survival factor S^2 which decreases with energy.

The present diffractive data are better described within the 'strong coupling' approach [7], and in this paper we shall give predictions for the LHC for this scenario. However, the possibility of the 'weak coupling' scenario is not completely excluded yet. Therefore, it is quite important to study the different channels of diffractive dissociation at the LHC in order to reach a final conclusion and to fix the parameters of the model for high-energy soft interactions. So the first motivation is the intrinsic interest in obtaining a reliable, self-consistent model for soft interactions, which may be illuminated by data from the LHC [8].

B. In turn, obtaining a reliable model will be of great value for predictions of the gross features of soft interactions. In particular, it is essential for understanding the structure of the underlying events at the LHC.

C. The third reason for studying soft interactions arises because it may not be an easy task to identify the production of a new object at the LHC when it is accompanied by hundreds of other particles emitted in the same event. For the detailed study of the new object, A , it may be better to select the few, very clean, events with the Large Rapidity Gaps (LRG) on either side of the new object, see, for example, [9, 10, 11, 12]. That is to observe the exclusive process $pp \rightarrow p + A + p$. In such a Central Exclusive Process (CEP) the mass of A can be measured with very good accuracy ($\Delta M_A \sim 1 - 2 \text{ GeV}$) by the missing-mass method by detecting the outgoing very forward protons. Moreover, a specific $J_z = 0$ selection rule [13] reduces the background and also greatly simplifies the spin-parity analysis of A . However, the CEP cross section is strongly suppressed by the small survival factor, $S^2 \ll 1$, of the rapidity gaps. Thus we need a reliable model of soft interactions to evaluate the corresponding value of S^2 [14]. Moreover, it is important to have a model which contains t -channel components of different size in order to evaluate the possible effects of the 'soft-hard factorisation' breaking. This is the subject of the following paper [15].

$$T_{\text{el}}(s, b) = i(1 - e^{-\Omega/2}) = \sum_{n=1}^{\infty} \overbrace{\left[\begin{array}{c} | \quad | \quad | \quad | \quad | \\ \Omega/2 \quad \Omega/2 \quad \dots \quad \Omega/2 \\ | \quad | \quad | \quad | \quad | \end{array} \right]}^{\text{Figure 1}}$$

Figure 1: The eikonal model of elastic scattering

2 Résumé of the eikonal formalism

2.1 Single-channel eikonal model

First, we briefly recall the relevant features of the single-channel eikonal model. That is, we focus on elastic unitarity. At high energy the position of the fast particle in the impact parameter, b , plane is to a good approximation frozen during the interaction, since the value of b is fixed by the orbital angular momentum $l = b\sqrt{s}/2$ of the incoming hadron. There is no mixture between the partial wave amplitudes with different l . The well known solution of the elastic unitarity equation,

$$2\text{Im} T_{\text{el}}(s, b) = |T_{\text{el}}(s, b)|^2 + G_{\text{inel}}(s, b), \quad (2)$$

may be written in terms of the phase shift δ_l as

$$S_{\text{el}} \equiv 1 + iT_{\text{el}} = e^{2i\delta_l}, \quad \text{that is } T_{\text{el}} = i(1 - e^{2i\delta_l}). \quad (3)$$

The presence of inelastic channels, given by G_{inel} in (2), leads to the phase δ_l having an imaginary part. That is, δ_l becomes a complex number. Moreover, at high energies we know that $\text{Re}T_{\text{el}}/\text{Im}T_{\text{el}}$ is small.

Now, in the framework of the eikonal model, the elastic amplitude,

$$T_{\text{el}} = i(1 - e^{-\Omega/2}) \quad (4)$$

is obtained by the sum of Regge-exchange diagrams, which is equivalent to the iteration of the elastic unitarity equation, (2), as shown in Fig. 1. In other words, s -channel elastic unitarity gives

$$\text{Im}T_{\text{el}}(s, b) = 1 - e^{-\Omega/2} \quad (5)$$

$$\sigma_{\text{el}}(s, b) = (1 - e^{-\Omega/2})^2, \quad (6)$$

$$\sigma_{\text{inel}}(s, b) = 1 - e^{-\Omega}, \quad (7)$$

where $\Omega(s, b) \geq 0$ is called the opacity (optical density) or eikonal¹; $\Omega/2$ plays the role of $-2i\delta_l$. It is the Fourier transform of the two-particle (s -channel) *irreducible* amplitude, $A(s, q_t)$. That is²

$$\Omega(s, b) = \frac{-i}{4\pi^2} \int d^2q_t A(s, q_t) e^{i\mathbf{q}_t \cdot \mathbf{b}}, \quad (8)$$

¹Sometimes $\Omega/2$ is called the eikonal.

²We use the bold face symbols \mathbf{q}_t and \mathbf{b} to denote vectors in the transverse plane.

where $q_t^2 = -t$, and where the amplitude is normalized by the relation $\sigma_{\text{tot}}(s) = \text{Im}T_{\text{el}}(s, t = 0)$. From (7), we see that $\exp(-\Omega(s, b))$ is the probability that no inelastic scattering occurs at impact parameter b .

After summing over b (that is, all partial waves) we obtain the total, elastic and inelastic cross sections

$$\sigma_{\text{tot}} = 2 \int d^2b \text{Im} T_{\text{el}}(s, b) = 2 \int d^2b (1 - e^{-\Omega/2}) \quad (9)$$

$$\sigma_{\text{el}} = \int d^2b |T_{\text{el}}(s, b)|^2 = \int d^2b (1 - e^{-\Omega/2})^2 \quad (10)$$

$$\sigma_{\text{inel}} = \int d^2b [2\text{Im} T_{\text{el}}(s, b) - |T_{\text{el}}(s, b)|^2] = \int d^2b (1 - e^{-\Omega}). \quad (11)$$

Below we neglect the imaginary part of Ω , apart from the contribution of secondary Reggeons to high-mass diffractive dissociation. At high energies, the ratio $\text{Re}T_{\text{el}}/\text{Im}T_{\text{el}}$ is small, and can be evaluated via a dispersion relation.

2.2 Inclusion of low-mass diffractive dissociation

So much for elastic diffraction. Now we turn to inelastic diffraction, which is a consequence of the *internal structure* of hadrons. Besides the pure elastic two-particle intermediate states shown in Fig. 1, there is the possibility of proton excitation, $p \rightarrow N^*$. As a rule such excitations are not included in the opacity Ω , but are treated separately.

This is simplest to describe at high energies, where the lifetime of the fluctuations of the fast proton is large, $\tau \sim E/m^2$, and during these time intervals the corresponding Fock states can be considered as ‘frozen’. Each constituent of the proton can undergo scattering and thus destroy the coherence of the fluctuations. As a consequence, the outgoing superposition of states will be different from the incident particle, and will most likely contain multiparticle states, so we will have *inelastic*, as well as elastic, diffraction.

To discuss inelastic diffraction, it is convenient to follow Good and Walker [16], and to introduce states ϕ_k which diagonalize the T matrix. Such eigenstates only undergo elastic scattering. Since there are no off-diagonal transitions,

$$\langle \phi_j | T | \phi_k \rangle = 0 \quad \text{for } j \neq k, \quad (12)$$

a state k cannot diffractively dissociate into a state j . We have noted that this is not, in general, true for hadronic states, which are not eigenstates of the S -matrix, that is of T . To account for the internal structure of the hadronic states, we have to enlarge the set of intermediate states, from just the single elastic channel, and to introduce a multichannel eikonal. We will consider such an example below, but first let us express the cross section in terms of the probability amplitudes F_k of the hadronic process proceeding via the various diffractive eigenstates³ ϕ_k .

³The exponent $\exp(-\Omega_k)$ describes the probability that the diffractive eigenstate ϕ_k is not absorbed in the interaction. Later we will see that the rapidity gap survival factors, S^2 , can be described in terms of such eikonal exponents.

Let us denote the orthogonal matrix which diagonalizes $\text{Im } T$ by a , so that

$$\text{Im } T = a T^D a^T \quad \text{with} \quad \langle \phi_j | T^D | \phi_k \rangle = T_k^D \delta_{jk}. \quad (13)$$

Now consider the diffractive dissociation of an arbitrary incoming state

$$|j\rangle = \sum_k a_{jk} |\phi_k\rangle. \quad (14)$$

The elastic scattering amplitude for this state satisfies

$$\langle j | \text{Im } T | j \rangle = \sum_k |a_{jk}|^2 T_k^D = \langle T^D \rangle, \quad (15)$$

where $T_k^D \equiv \langle \phi_k | T^D | \phi_k \rangle$ and where the brackets of $\langle T^D \rangle$ mean that we take the average of T^D over the initial probability distribution of diffractive eigenstates. After the diffractive scattering described by T_{fj} , the final state $|f\rangle$ will, in general, be a different superposition of eigenstates from that of $|j\rangle$, which was shown in (14). At high energies we may neglect the real parts of the diffractive amplitudes. Then, for cross sections at a given impact parameter b , we have

$$\begin{aligned} \frac{d\sigma_{\text{tot}}}{d^2b} &= 2 \text{Im} \langle j | T | j \rangle = 2 \sum_k |a_{jk}|^2 T_k^D = 2 \langle T^D \rangle \\ \frac{d\sigma_{\text{el}}}{d^2b} &= |\langle j | T | j \rangle|^2 = \left(\sum_k |a_{jk}|^2 T_k^D \right)^2 = \langle T^D \rangle^2 \\ \frac{d\sigma_{\text{el} + \text{SD}}}{d^2b} &= \sum_k |\langle \phi_k | T | j \rangle|^2 = \sum_k |a_{jk}|^2 (T_k^D)^2 = \langle (T^D)^2 \rangle. \end{aligned} \quad (16)$$

It follows that the cross section for the single diffractive dissociation of a proton,

$$\frac{d\sigma_{\text{SD}}}{d^2b} = \langle (T^D)^2 \rangle - \langle T^D \rangle^2, \quad (17)$$

is given by the statistical dispersion in the absorption probabilities of the diffractive eigenstates. Here the average is taken over the components k of the incoming proton which dissociates. If the averages are taken over the components of both of the incoming particles, then in (17) we must introduce a second index on T^D , that is T_{ik}^D , and sum over k and i . In this case the sum is the cross section for single and double dissociation.

At first sight, enlarging the number of eigenstates $|\phi_i\rangle$ we may include even high-mass proton dissociation. However here we face the problem of double counting when the partons originating from dissociation of the beam and ‘target’ initial protons overlap in rapidities. For this reason high-mass dissociation is usually described by ‘enhanced’ multi-Pomeron diagrams. The first and simplest is the triple-Pomeron graph, see Fig. 5 below.

3 Triple-Regge analysis accounting for absorptive effects

The total and elastic proton-proton cross sections are usually described in terms of an eikonal model, which automatically satisfies s -channel elastic unitarity. To account for the possibility of excitation of the initial proton, that is for two-particle intermediate states with the proton replaced by N^* , we use the Good-Walker formalism [16]. Already at Tevatron energies the absorptive correction to the elastic amplitude, due to elastic eikonal rescattering, is not negligible; it is about -20% in comparison with the simple one Pomeron exchange. After accounting for low-mass proton excitations (that is N^* 's in the intermediate states) the correction becomes twice larger (that is, about -40%). Indeed, the possibility of proton excitation means that we have to include additional inelastic channels which were not accounted for in the irreducible amplitude A of (8). This enlarges the probability of absorption for the elastic channel, that is the effective opacity Ω . In terms of the Good-Walker formalism, the stronger absorption follows from the inequality⁴

$$\langle \Omega_k e^{-\Omega_k} \rangle < \langle \Omega_k \rangle \langle e^{-\Omega_k} \rangle, \quad (18)$$

where we average over the diffractive (Good-Walker) eigenstates.

Next, in order to describe high-mass diffractive dissociation, $d\sigma_{SD}/dM^2$, we have to include an extra factor of 2 from the AGK cutting rules [17]. Thus, the absorptive effects in the triple-Regge domain are expected to be quite large. The previous triple-Regge analyses (see, for example, [18]) did not allow for absorptive corrections and the resulting triple-Regge couplings must be regarded, not as bare vertices, but as effective couplings embodying the absorptive effects [19]. Since the inelastic cross section (and, therefore, the absorptive corrections) expected at the LHC are more than twice as large as that observed at fixed-target and CERN-ISR energies, the old triple-Regge vertices cannot be used to predict the diffractive cross sections at the LHC.

Thus, it is necessary to perform a new triple-Regge analysis that includes the absorptive effects explicitly. Such an analysis has recently been performed [7] using the fixed-target FNAL, CERN-ISR and Tevatron data that are available in the triple-Regge region. The ‘ PPP ’, ‘ PPR ’, ‘ RRP ’, ‘ RRR ’ and $\pi\pi P$ contributions, were included assuming either the ‘strong’ or ‘weak’ coupling scenarios for the behaviour of the triple-Pomeron vertex. To account for the absorptive corrections a two-channel (Good-Walker) eikonal model was used, which describes well the total, σ_{tot} , and elastic, $d\sigma_{el}/dt$, pp and $\bar{p}p$ cross sections.

In the ‘strong’ coupling case, a good $\chi^2/\text{DoF}=167/(210-8)=0.83$ was obtained. In comparison with the old triple-Regge analysis [18], a twice larger relative contribution of the ‘ PPR ’ term was found. This is mainly due to the inclusion of the higher-energy Tevatron data in the analysis.

⁴When we go from a single- to a many-channel eikonal, we may write $\Omega_k = \langle \Omega \rangle + \delta_k$ with $\langle \delta_k \rangle = 0$. It follows that $\langle \Omega_k e^{-\Omega_k} \rangle = \langle \Omega \rangle \langle e^{-\Omega_k} \rangle + \langle \delta_k e^{-\delta_k} \rangle e^{-\langle \Omega \rangle}$ which, since the second term is negative, is less than $\langle \Omega \rangle \langle e^{-\Omega_k} \rangle$.

Since the absorptive effects are included explicitly, the extracted values of the triple-Reggeon vertices are now much closer to the *bare* triple-Regge couplings. In particular, the value

$$g_{PPP} \equiv \lambda g_N, \quad \text{where } \lambda \simeq 0.2 \quad (19)$$

is consistent with a reasonable extrapolation of the perturbative BFKL Pomeron vertex to the low scale region [20]; here g_N is the Pomeron-proton coupling. Note also that these values of the ‘*PPP*’ and ‘*PPR*’ vertices allow a good description of the HERA data [21] on inelastic J/ψ photoproduction, $\gamma p \rightarrow J/\psi + Y$, where the screening corrections are rather small.

The ‘weak’ coupling scenario leads to a larger $\chi^2/\text{DoF}=1.4$ and to a worse description of the $\gamma p \rightarrow J/\psi + Y$ process at the lowest values of t . At the LHC energy the ‘weak’ coupling fit predicts about 3 times smaller inclusive cross section $d\sigma_{\text{SD}}/dt dM^2$ at $\xi = M^2/s = 0.01$ and low t in comparison with that predicted in the ‘strong’ coupling case.

4 Model with a complete set of multi-Pomeron vertices

Note that the effects due to the triple-Pomeron vertex (19) are rather large. Indeed, the contribution caused by such vertices is enhanced by the logarithmically large phase space available in rapidity. In particular, the total cross section of high-mass dissociation is roughly⁵ of the form

$$\sigma_{\text{SD}} = \int \frac{M^2 d\sigma_{\text{SD}}}{dM^2} \frac{dM^2}{M^2} \sim \lambda \ln s \sigma_{\text{el}}, \quad (20)$$

where λ reflects the suppression of high-mass dissociation in comparison with elastic scattering and the $\ln s$ factor comes from the integration $\int dM^2/M^2 \sim \ln s$. Thus actually we deal with the parameter $\lambda \ln s \gtrsim 1$ at collider energies. For each fixed rapidity interval the probability of high-mass dissociation (or, in other words, the contribution due to the triple-Pomeron vertex) is relatively small. However the cumulative effect in the complete interaction amplitude is enhanced by the large phase space available in rapidity.

As a consequence, the contribution of the corresponding, so-called ‘enhanced’, diagrams, with a few vertices, is not negligible. Moreover, we cannot expect that more complicated multi-Pomeron interactions, driven by the g_m^n vertices, which describe the transition of n to m Pomerons of Fig. 2, will not affect the final result. It looks more reasonable to assume that $g_m^n \propto \lambda^{n+m}$ than to assume that $g_m^n = 0$ for any $n + m > 3$. Thus we need a model which accounts for the possibility of multi-Pomeron interactions (with arbitrary n and m).

In this paper we extend and develop the *partonic* approach of Ref. [22]. While the eikonal formalism describes the rescattering of the incoming fast particles, the enhanced multi-Pomeron diagrams represent the rescattering of the intermediate partons in the ladder (Feynman diagram) which describes the Pomeron-exchange amplitude.

⁵Here, for simplicity, we assume an essentially flat energy dependence, $\sigma \sim s^\epsilon$ with $\epsilon \ln s < 1$.

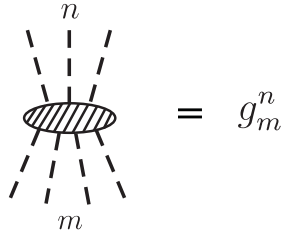


Figure 2: A multi-Pomeron vertex

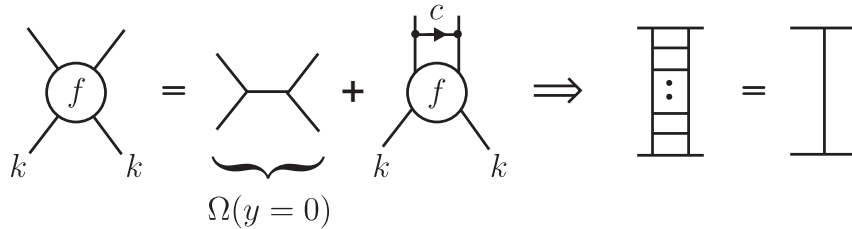


Figure 3: The evolution of the elastic bare Pomeron amplitude, $\Omega_k(y, b)$.

Indeed, we start with the generation of ladder-type structure of ‘elastic’ bare Pomeron exchange amplitude. It may be generated by the evolution equation [23] (in rapidity, y , space)

$$\frac{d\Omega(y, b)}{dy} = \left(\Delta + \alpha' \frac{d^2}{d^2b} \right) \Omega(y, b), \quad (21)$$

where b is the two-dimensional vector in impact parameter space. Δ is the probability to emit new intermediate partons (denoted c) within unit rapidity interval; it is analogous to the splitting function of DGLAP evolution. The impact parameter of parton c is not frozen in the evolution. At each step b can be changed by a constant amount Δb in any direction, leading to the diffusion represented by the second term on the right-hand side of (21) where α' plays the role of the diffusion coefficient [24]. The evolution is shown symbolically in Fig. 3. The solution of (21) is

$$\Omega(y, b) = \Omega_0 \exp(y\Delta - b^2/4\alpha'y)/4\pi\alpha'y. \quad (22)$$

It represents the opacity (at point y, b), corresponding to the incoming particle placed at $b = 0$ and $y = 0$.

It may be helpful to explain why (21) was written in terms of the opacity Ω . First we note that the discontinuity of the amplitude generated by (21) does not contain a two-particle s -channel intermediate state; it corresponds to a pure inelastic high multiplicity process, see Fig. 4. Due to elastic unitarity, (2) this inelastic interaction leads to elastic pp scattering. Thus we have to put the solution of (21) into the eikonal formulae of (5)-(7), as it does not contain two-particle s -channel states.



Figure 4: A pure inelastic high multiplicity process

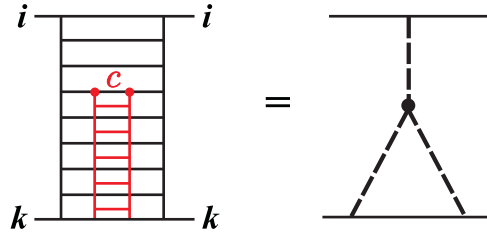


Figure 5: The ladder structure of the triple-Pomeron amplitude.

In momentum space the solution (22) corresponds to the amplitude

$$A(s, t) = A_0 s^{1+\Delta+\alpha' t}. \quad (23)$$

That is to the bare Pomeron exchange amplitude, where the Pomeron trajectory has intercept $\alpha(0) = 1 + \Delta$ and slope α' .

A multi-Pomeron enhanced contribution arises from the absorption of intermediate s -channel partons c during the evolution of Ω in y . The simplest example is the triple-Pomeron diagram in which parton c undergoes an extra rescattering with the target parton k , as shown in Fig. 5. Allowing for many rescatterings, we have to sum over different numbers of ladders between partons c and k . Assuming an eikonal form for the multi-Pomeron-proton vertex, it is natural to replace (21) by

$$\frac{d\Omega_k}{dy} = e^{-\lambda\Omega_k/2} \left(\Delta + \alpha' \frac{d^2}{d^2b} \right) \Omega_k(y, b) \quad (24)$$

where the ‘opacity’ Ω_k describes the transparency of the target k . As we are dealing with the elastic *amplitude* we use $e^{-\lambda\Omega_k/2}$ and not $e^{-\lambda\Omega_k}$. The coefficient λ arises since parton c will have a different absorption cross section from that of eigenstate i . Naively, we may assume that the beam i contains a number $1/\lambda$ of partons. The factor $e^{-\lambda\Omega_k/2}$ generates multi-Pomeron vertices of the form

$$g_m^n = n \cdot m \cdot \lambda^{n+m-2} g_N / 2 \quad \text{for } n + m \geq 3. \quad (25)$$

where g_m^n is defined in Fig. 2. Even though $\lambda \simeq 0.25$, the role of the factor $e^{-\lambda\Omega_k/2}$ is not negligible, since the suppression effect is accumulated throughout the evolution. For instance,

if $\lambda \ll 1$ the full absorptive correction is given by the product $\lambda\Omega Y/2$, where the small value of λ is compensated by the large rapidity interval Y .

In terms of Regge diagrams, (24) sums up the system of fan diagrams in which any number m of “lower” Pomerons couples to a fan vertex g_m^1 . Such multi-Pomeron diagrams are called “enhanced”, since their contribution is enhanced, in comparison with the eikonal diagrams, by the large available rapidity interval Y . In order to include the rescattering with the beam i we replace (24) by

$$\frac{d\Omega_k(y, b)}{dy} = e^{-\lambda(\Omega_k(y, b) + \Omega_i(y', b))/2} \left(\Delta + \alpha' \frac{d^2}{d^2b} \right) \Omega_k(y, b), \quad (26)$$

The final term in the exponent is the opacity of the beam i , which depends on the rapidity interval $y' = Y - y$, with $Y = \ln s$. The equation for the opacity Ω_i has an analogous form

$$\frac{d\Omega_i(y', b)}{dy'} = e^{-\lambda(\Omega_i(y', b) + \Omega_k(y, b))/2} \left(\Delta + \alpha' \frac{d^2}{d^2b} \right) \Omega_i(y', b), \quad (27)$$

in which we now evolve in the opposite direction starting from the boundary condition $\Omega(y' = 0)$ at $y = Y$.

Recall that the fit to the data in the triple-Reggeon domain indicated a very small (consistent with zero) t -slope of all the triple-Reggeon vertices [7, 18]. Thus, as the size of the multi-Reggeon vertices are negligible in comparison with the size of the incoming hadron, we may write the absorptive corrections (that is, the exponential factors on the right-hand-side of (26,27)) such that the opacities Ω_i, Ω_k are taken at the same point in the impact parameter plane b .

Since the intermediate parton may be absorbed by the interaction with the particles (partons) from the wave function of both the beam or target hadron, we now need to solve the two equations, (26) and (27). This is done iteratively. Moreover, note that the opacities Ω now depend on two vectors in impact parameter space - the separation \mathbf{b}_1 between the position of the intermediate parton c and the beam hadron, and the separation \mathbf{b}_2 between c and the target hadron. The argument b in (26,27) now symbolically denotes both \mathbf{b}_1 and \mathbf{b}_2 . The resulting solution $\Omega(y, \mathbf{b})$ is then used in the eikonal formulae for the elastic amplitude, giving

$$T_{\text{el}}(\mathbf{b}) = 1 - \exp(-\Omega(\mathbf{b} = \mathbf{b}_1 - \mathbf{b}_2)/2). \quad (28)$$

A more detailed description of the amplitude, and the cross sections of the different diffractive processes can be found in Ref. [22].

4.1 Multi-components in both the s - and t -channels

As mentioned above, as in [22], we use three diffractive components in the s -channel. In other words, we use a 3-channel eikonal for the rescattering of fast particles. The transverse size squared of each eigenstate is proportional to the corresponding absorptive cross section; $R_i^2 \propto \sigma_i$. That is, we assume that the parton density at the origin is the same for each eigenstate. The

shape of the Pomeron-nucleon vertex is parametrised by the form factor $V(t) = e^{d_2 t} / (1 - t/d_1)^2$, whose Fourier transform, $V(\mathbf{b})$, plays the role of the initial conditions for $\Omega(y = 0, \mathbf{b})$. However, now, we allow for a non-zero slope ($\alpha' \neq 0$) of the (bare) Pomeron trajectory.

A major development, of the model of [22], is that we use four different t -channel states, which we label a : one for the secondary Reggeon (R) trajectory and three Pomeron states (P_1, P_2, P_3) to mimic the BFKL diffusion in the logarithm of parton transverse momentum, $\ln(k_t)$ [25]. To be precise, since the BFKL Pomeron [26] is not a pole in the complex j -plane, but a branch cut, we approximate the cut by three t -channel states of a different size. The typical values of k_t in each of the three states is about $k_{t1} \sim 0.5$ GeV, $k_{t2} \sim 1.5$ GeV and $k_{t3} \sim 5$ GeV. Thus the system of evolution equations (26,27) is replaced by⁶

$$\frac{d\Omega_k^a(y, \mathbf{b}_1, \mathbf{b}_2)}{dy} = e^{-\lambda[\bar{\Omega}_k^a(y, \mathbf{b}_1, \mathbf{b}_2) + \bar{\Omega}_i^a(y', \mathbf{b}_1, \mathbf{b}_2)]/2} \left(\Delta^a + \alpha'_a \frac{d^2}{d^2 b_1} \right) \Omega_k^a(y, \mathbf{b}_1, \mathbf{b}_2) + V_{aa'} \Omega_k^{a'}, \quad (29)$$

$$\frac{d\Omega_i^a(y', \mathbf{b}_1, \mathbf{b}_2)}{dy'} = e^{-\lambda[\bar{\Omega}_k^a(y, \mathbf{b}_1, \mathbf{b}_2) + \bar{\Omega}_i^a(y', \mathbf{b}_1, \mathbf{b}_2)]/2} \left(\Delta^a + \alpha'_a \frac{d^2}{d^2 b_2} \right) \Omega_i^a(y', \mathbf{b}_1, \mathbf{b}_2) + V_{aa'} \Omega_i^{a'}, \quad (30)$$

where $\Delta^a = \alpha(0) - 1$ and $\alpha'_a = \alpha'_P$ for $a = P_1, P_2, P_3$, while for the secondary Reggeon, ($a = R$), which is built of quarks, we take $\Delta^R = \alpha_R(0) = 0.6$ and $\alpha'_R = 0.9$ GeV⁻², so that the last term $V_{RR} \Omega^R$ is diagonal with $V_{RR} = -1$ to account for the spin $\frac{1}{2}$ nature of quarks. The key parameters which drive the evolution are the intercepts Δ and the slopes α' . In general, each component a may have different values of Δ_a and α'_a . We discuss the values in Section 5.

In the exponents, the opacities $\bar{\Omega}_i$ ($\bar{\Omega}_k$) are actually the sum of the opacities $\Omega_i^{a'}$ ($\Omega_k^{a'}$) with corresponding coefficients. Namely

$$\begin{aligned} \bar{\Omega}^{P_1} &= \Omega^{P_1} + \Omega^{P_2} v_{PP} + \Omega^R v_{PR} \\ \bar{\Omega}^{P_2} &= \Omega^{P_2} + \Omega^{P_1} v_{PP} + \Omega^{P_3} v'_{PP} \\ \bar{\Omega}^{P_3} &= \Omega^{P_3} + \Omega^{P_2} v'_{PP} \\ \bar{\Omega}^R &= \Omega^{P_1} v_{RP} + \Omega^R v_{RR}. \end{aligned} \quad (31)$$

We chose $v_{PP} = (1/3)^2$ since, at the leading order, the probability of interaction of two components of different size (k_t) is proportional to the ratio $(k_{t2}/k_{t1})^2$. We take $v'_{PP} = 1/27$ since the third (smallest size) component collects *all* the higher k_t contributions, and therefore here the mean value of k_t is larger. For the screening of the secondary Reggeon by the Pomeron we take just the colour factor $v_{RP} = C_F/C_A = (4/9)$, as we assume that the secondary Reggeon is composed of a t -channel quark-antiquark pair. Finally the factors $v_{PR} = 1.8$ and $v_{RR} = 4$

⁶Strictly speaking both opacities Ω_i and Ω_k depend on both subscripts i and k . Here we keep only one subscript to distinguish the parent hadron for each active parton (gluon).

were tuned to give a reasonable reproduction of the secondary Reggeon contributions to the available $pp \rightarrow p + X$ data⁷.

The transition factors $V_{aa'}$ between the different t -channel components are fixed by the properties of the BFKL equation. The only non-zero factors, apart from $V_{RR} = -1$, are

$$V_{P_1 P_2} = \rho^{P_2} v_{PP}, \quad V_{P_2 P_1} = \rho^{P_1} v_{PP}, \quad V_{P_2 P_3} = \rho^{P_3} v'_{PP}, \quad V_{P_3 P_2} = \rho^{P_2} v'_{PP}, \quad (32)$$

where

$$\rho_{ik}^a = \Delta^a e^{-\lambda(\bar{\Omega}_k^a(y,b) + \bar{\Omega}_i^a(y',b))/2}. \quad (33)$$

ρ^a is the density of partons emitted in the rapidity evolution of the t -channel component a . The remaining transition factors were set to zero. That is

$$V_{P_3 P_1} = V_{P_1 P_3} = 0, \quad V_{Ra'} = V_{aR} = 0, \quad \text{and} \quad V_{aa'} = 0 \quad \text{for} \quad a = a'. \quad (34)$$

For each Good-Walker s -channel component (i, k) , the initial conditions are fixed by the parton (matter) distribution in the corresponding diffractive eigenstate

$$\Omega_i^a(y=0, \mathbf{b}) = \frac{\beta_i(\mathbf{b})\beta_0}{4\pi} = \frac{\beta_0}{4\pi^2} \int e^{i\mathbf{q}\cdot\mathbf{b}} \beta_i(t) d^2 q_t, \quad (35)$$

where $\beta_i(t) = \gamma_i \beta(\gamma_i t)$. The parametrisation $\beta(t) = \beta_0 e^{d_2 t} / (1-t/d_1)^2$ was used for the Pomeron, while for the secondary Reggeon we chose the Gaussian form $\beta(t) = \beta_R e^{d_R t}$.

The relative couplings (and the corresponding size) of the components were taken to (a) reproduce the cross section of low-mass dissociation measured at the CERN-ISR [27], and (b) to make all three components quite different from each other; $\gamma_1 = 1.80$, $\gamma_2 = 0.82$, $\gamma_3 = 0.38$. All the coefficients in the decomposition $|p\rangle = \sum a_i |\phi_i\rangle$ are taken to be $a_i = 1/\sqrt{3}$ (with $i = 1, 2, 3$).

To avoid possible double counting, and to fix the boundary between the ‘low’ and ‘high’ mass dissociation, we introduce a threshold $\Delta y = 1.5$ in rapidity for the actual start of the evolution of (29,30). That is we start the evolution at $y = \Delta y = 1.5$ and not at $y = 0$. Hence the available rapidity interval becomes $\delta Y = \ln(s) - 2\Delta y$. Proton excitation (dissociation) which covers a rapidity interval larger than Δy (i.e. $\ln(M^2/s_0) > 1.5$) is called ‘high-mass dissociation’.

It is natural to separate the different contributions in terms of rapidity, since in QCD the interference between the different diagrams for gluon radiation leads to angular (rapidity) ordering of emitted gluons, at least to leading log accuracy⁸.

Note that the initial condition (35) is only valid for the secondary Reggeon and for the large size Pomeron component ($a = P_1$). For the smaller size Pomeron components we use

$$\Omega_i^{P_2}(y=0, \mathbf{b}) = \Omega_i^{P_1}(y=0, \mathbf{b}) v_{PP} \quad \text{and} \quad \Omega_i^{P_3}(y=0, \mathbf{b}) = \Omega_i^{P_1}(y=0, \mathbf{b}) v_{PP} v'_{PP}. \quad (36)$$

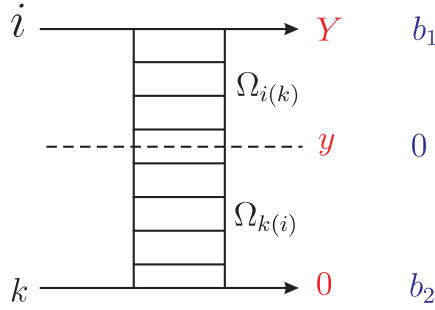


Figure 6: The irreducible amplitude $F_{ik}(Y, \mathbf{b})$ of a high energy interaction.

4.2 Total and differential cross section formulae

To calculate the elastic amplitude we need the s -channel two-particle *irreducible* amplitudes for the scattering of the various diffractive eigenstates i and k , for given separations $\mathbf{b} = \mathbf{b}_1 - \mathbf{b}_2$ between the incoming protons. These are given by

$$F_{ik}(Y, \mathbf{b}) = \frac{1}{\beta_0^2} \sum_a \int \Omega_{ik}^a(y, \mathbf{b}_1, \mathbf{b}_2) \Omega_{ik}^a(Y - y, \mathbf{b}_1, \mathbf{b}_2) d^2 b_1 d^2 b_2 \delta^{(2)}(\mathbf{b}_1 - \mathbf{b}_2 - \mathbf{b}) \quad (37)$$

where $Y = \ln s$, see Fig. 6. Note that there is no integral⁹ over y . The convolution may be calculated at any rapidity y , leading to the same result. Given this effective ‘ ik eikonal’, we can calculate the cross sections (analogously to (5)-(7)). We obtain

$$\sigma_{\text{tot}}(Y, \mathbf{b}) = 2 \sum_{i,k} |a_i|^2 |a_k|^2 \int \left(1 - e^{F_{ik}(Y, \mathbf{b})/2}\right) d^2 b, \quad (38)$$

$$\frac{d\sigma_{\text{el}}(Y, \mathbf{b})}{dt} = \frac{1}{4\pi} \left[\int d^2 b e^{i\mathbf{q}_t \cdot \mathbf{b}} \sum_{i,k} |a_i|^2 |a_k|^2 \left(1 - e^{F_{ik}(Y, \mathbf{b})/2}\right) \right]^2 \quad (39)$$

where $t = -q_t^2$, and

$$\sigma_{\text{el}}(Y, \mathbf{b}) = \int d^2 b \left[\sum_{i,k} |a_i|^2 |a_k|^2 \int \left(1 - e^{F_{ik}(Y, \mathbf{b})/2}\right) \right]^2. \quad (40)$$

⁷Note that all the opacities in the absorptive exponents are multiplied by $\lambda = 0.25$. Thus, the value of the product $\lambda v_{RR} = 1$ is not large.

⁸Therefore it will be interesting and important to measure the single diffractive cross section, not only in the usual form $d\sigma_{\text{SD}}/dM^2$, but also in the form $d\sigma_{\text{SD}}/d\eta$, where η denotes the position of the edge of the rapidity gap. This may be possible using the forward shower counters proposed in [28].

⁹The integral over y gives the multiplicity.

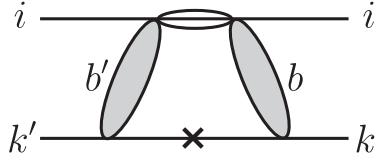


Figure 7: The symbolic diagram for (41) for low-mass dissociation of the ‘beam’ diffractive eigenstate i .

4.3 Low-mass diffractive dissociation

For low-mass excitation of the beam proton we obtain

$$\frac{d\sigma_{\text{el+SD}}(Y, \mathbf{b})}{dt} = \frac{1}{4\pi} \sum_{i,k,k'} |a_i|^2 |a_k|^2 |a_{k'}|^2 \times$$

$$\times \left[\int d^2b' e^{-i\mathbf{q}_t \cdot \mathbf{b}'} \left(1 - e^{F_{ik'}(Y, \mathbf{b}')/2} \right) \right] \left[\int d^2b e^{i\mathbf{q}_t \cdot \mathbf{b}} \left(1 - e^{F_{ik}(Y, \mathbf{b})/2} \right) \right], \quad (41)$$

which has the symbolic structure shown in Fig. 7.

Strictly speaking, we may need a different diagonalisation matrix a of (13) for the different t -channel exchanges. However, if the main difference between the diffractive eigenstates is due to the size and the impact parameter structure of the state, which is frozen for a fast hadron during the interaction, then it is justified to use the same eigenstates for any t -channel exchange, Ω^a .

4.4 High-mass diffractive dissociation

The expression for the high-mass excitation is more complicated. The cross section for beam particle diffractive dissociation (with the gap up to y) can be written using (5)-(7). Diffractive dissociation may be considered as the elastic scattering of intermediate parton c caused by its absorption on the target, which is described by the factor $\exp(-\lambda\bar{\Omega}_k/2)$.

Thus, in each impact parameter point \mathbf{b} the cross section for single dissociation is proportional to (i) the elastic $c-k$ cross section $(1 - \exp(-\lambda\bar{\Omega}_k(y, \mathbf{b})/2))^2$; (ii) to the probability to find the intermediate parton c in the interval dy , that is $\Delta \exp(-\lambda\bar{\Omega}_i/2 - \lambda\bar{\Omega}_k/2)$; (iii) to the amplitude Ω_i of the parton c -beam interaction; (iv) to the gap survival factor $S^2(\mathbf{b}) = \exp(-\Omega(Y, \mathbf{b}))$ ($Y = \ln s$). The resulting cross section reads

$$\frac{d\sigma_{\text{SD}}}{dy} = N \int (1 - e^{-\lambda\Omega_k(y, \mathbf{b}_1, \mathbf{b}_2)/2})^2 \Delta e^{-\lambda\Omega_i(Y-y, \mathbf{b}_1, \mathbf{b}_2)/2 - \lambda\Omega_k(y, \mathbf{b}_1, \mathbf{b}_2)/2} \times$$

$$\times \Omega_i(Y - y, \mathbf{b}_1, \mathbf{b}_2) S_{ik}^2(|\mathbf{b}_1 - \mathbf{b}_2|) d^2b_1 d^2b_2, \quad (42)$$

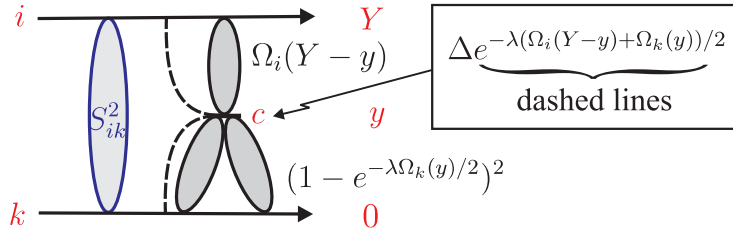


Figure 8: The symbolic diagram for (42) for high-mass dissociation of the ‘beam’ diffractive eigenstate i .

where \mathbf{b}_1 (\mathbf{b}_2) are the coordinates in the impact parameter plane with respect to the beam (target) hadron. The normalisation factor N is specified in (44). The gap survival probability¹⁰

$$S_{ik}^2(\mathbf{b}) = \exp(-F_{ik}(\mathbf{b})) . \quad (43)$$

The symbolic structure of (42), for high-mass single dissociation, is shown in Fig. 8.

Accounting for the different Good-Walker eigenstates and the different states in t -channel we obtain

$$\begin{aligned} \frac{M^2 d\sigma_{SD}}{dM^2} &= \sum_i |a_i|^2 \int \left| \sum_k |a_k|^2 \sum_a T_{ik}^a(y, \mathbf{b}_1, \mathbf{b}_2) \sqrt{\rho_{ik}^a(y, \mathbf{b}_1, \mathbf{b}_2)} S_{ik}(|\mathbf{b}_1 - \mathbf{b}_2|) \right|^2 \times \\ &\times \Omega_i^a(Y - y, \mathbf{b}_1, \mathbf{b}_2) d^2 b_1 d^2 b_2 / \beta_0^2 , \end{aligned} \quad (44)$$

where the parton density ρ_{ik}^a is defined by eq.(33) and, neglecting the secondary reggeon contribution, the elastic $c - k$ amplitude

$$T_{ik}^a(y, \mathbf{b}_1, \mathbf{b}_2) = \left(1 - e^{-\lambda \bar{\Omega}_k^a(y, \mathbf{b}_1, \mathbf{b}_2)/2} \right) . \quad (45)$$

For the secondary Reggeon, the real part may be large: note that $\alpha_{f_2}(\langle t \rangle) \sim 0.2$. To allow for this, and since, that besides the f_2 -trajectory with vacuum quantum numbers, there exists also ω , ρ and a_2 exchange, we enlarge the contribution due to Ω^R by increasing the values of the effective triple-Reggeon couplings g_{PPR} , g_{RRP} , g_{RRR} as compared to those coming from the absorptive opacities (31). So we use (45) for $a = P_2$ or P_3 . On the other hand, for $a = P_1$ or R we use, respectively,

$$T_{ik}^{P_1}(y, \mathbf{b}_1, \mathbf{b}_2) = \sqrt{\left(1 - e^{-\lambda \bar{\Omega}_k^{P_1}(y, \mathbf{b}_1, \mathbf{b}_2)/2} \right)^2 + r_{RRP} \left(1 - e^{-\lambda \Omega_k^R(y, \mathbf{b}_1, \mathbf{b}_2) v_{PR}/2} \right)^2} . \quad (46)$$

¹⁰Strictly speaking, when calculating the gap survival probability in each particular case, we only have to account for the possibility of rescattering which produces secondaries within the gap interval. That is, in (43) we should not put the whole irreducible amplitude $F_{ik}(\mathbf{b})$, but, instead, part of it; since the contribution from the processes with a gap in the same (or a larger) rapidity interval does not change qualitatively the structure of the diffractive dissociation event. In the present computations we neglect this effect. This means that actually the gap survival probabilities, and the true cross sections of diffractive dissociation, should be a bit larger.

and

$$T_{ik}^R(y, \mathbf{b}_1, \mathbf{b}_2) = \sqrt{\left(1 - e^{-\lambda\Omega'_k(y, \mathbf{b}_1, \mathbf{b}_2)/2}\right)^2 + r_{RRR} \left(1 - e^{-\lambda\Omega_k^R(y, \mathbf{b}_1, \mathbf{b}_2)v_{RR}/2}\right)^2}. \quad (47)$$

where $\Omega' = r_{PPR}\Omega^{P_1} + \Omega^R v_{RR}$. We take $r_{RRP} = r_{PPR} = 3$, $r_{RRR} = 9$ to reproduce the available data in the CERN-ISR to Tevatron energy range.

The slope of the diffractive dissociation cross section, $B_{SD} = d[\ln(d\sigma_{SD}/dM^2)]/dt$ at $t = 0$, can be calculated as the mean value of \mathbf{b}_2^2 – the separation of the intermediate parton c from the target hadron

$$B_{SD} = \sum_i |a_i|^2 \int \left| \sum_k |a_k|^2 \sum_a T_{ik}^a(y, \mathbf{b}_1, \mathbf{b}_2) \sqrt{\rho_{ik}^a(y, \mathbf{b}_1, \mathbf{b}_2)} S_{ik}(|\mathbf{b}_1 - \mathbf{b}_2|) \right|^2 \times \\ \times \mathbf{b}_2^2 \Omega_i^a(Y - y, \mathbf{b}_1, \mathbf{b}_2) \frac{d^2 b_1 d^2 b_2}{\beta_0^2} \left[\frac{M^2 d\sigma_{SD}}{dM^2} \right]^{-1}. \quad (48)$$

4.5 Central exclusive production

Central Exclusive Diffractive (CED) production of a system with mass squared $M^2 = \xi_1 \xi_2 s$ with the large rapidity gaps either side, which is sometimes called the Double-Pomeron-Exchange (DPE) process, has a cross section given by

$$\frac{\xi_1 \xi_2 d\sigma_{CED}}{d\xi_1 d\xi_2} = \sum_{a, a'} \int \left| \sum_{i, k} E_i^{a'} E_k^a \Omega^{aa'}(y_1, y_2, \mathbf{b}'_1, \mathbf{b}_2) S_{ik} \right|^2 d^2 b_1 d^2 b_2 d^2 b'_2 / \beta_0^2, \quad (49)$$

where

$$E_i^{a'} = |a_i|^2 T_{ik}^{a'}(Y - y_1, \mathbf{b}_1, \mathbf{b}'_2) \sqrt{\rho_{ik}^{a'}(Y - y_1, \mathbf{b}_1, \mathbf{b}'_2)}, \quad (50)$$

$$E_k^a = |a_k|^2 T_{ki}^a(y_2, \mathbf{b}'_1, \mathbf{b}_2) \sqrt{\rho_{ik}^a(y_2, \mathbf{b}'_1, \mathbf{b}_2)} \quad (51)$$

are the probability amplitudes for elastic scattering of the intermediate parton c (c') on the beam (target) eigenstate i (k). The coordinates of parton c (c') are \mathbf{b}_1 and \mathbf{b}'_2 (\mathbf{b}'_1 and \mathbf{b}_2) with respect to the beam and the target proton respectively; that is, $\mathbf{b}'_1 = \mathbf{b}_1 - \mathbf{b}'_2 + \mathbf{b}_2$. The momentum fractions ($\xi_i = 1 - x_{L,i}$) of the incoming protons, transferred across the gaps, are $\xi_1 = e^{-(Y-y_1)}$ and $\xi_2 = e^{-y_2}$. The gap survival factor $S_{ik}(b = |\mathbf{b}_1 - \mathbf{b}'_2|)$ is given by (43).

The amplitude of the interaction of partons c and c' , $\Omega^{aa'}(y_1, y_2, \mathbf{b}'_2, \mathbf{b}_2)$, is obtained by the solution of the evolution (29), which *starts* from the initial condition $\Omega^a(y = y_2) = \delta^{(2)}(\mathbf{b}'_2 - \mathbf{b}_2)$. That is, it *starts* from one parton at rapidity y_2 placed at coordinate \mathbf{b}_2 in t -channel state a , and *finishes* at the point y_1, \mathbf{b}'_2 in the state a' ; note $y_1 > y_2$. After the usual solution of (29,30), the evolution (29) was performed in the known “background” fields $\overline{\Omega}_k^a, \overline{\Omega}_i^a$ to account for the absorption of intermediate partons.

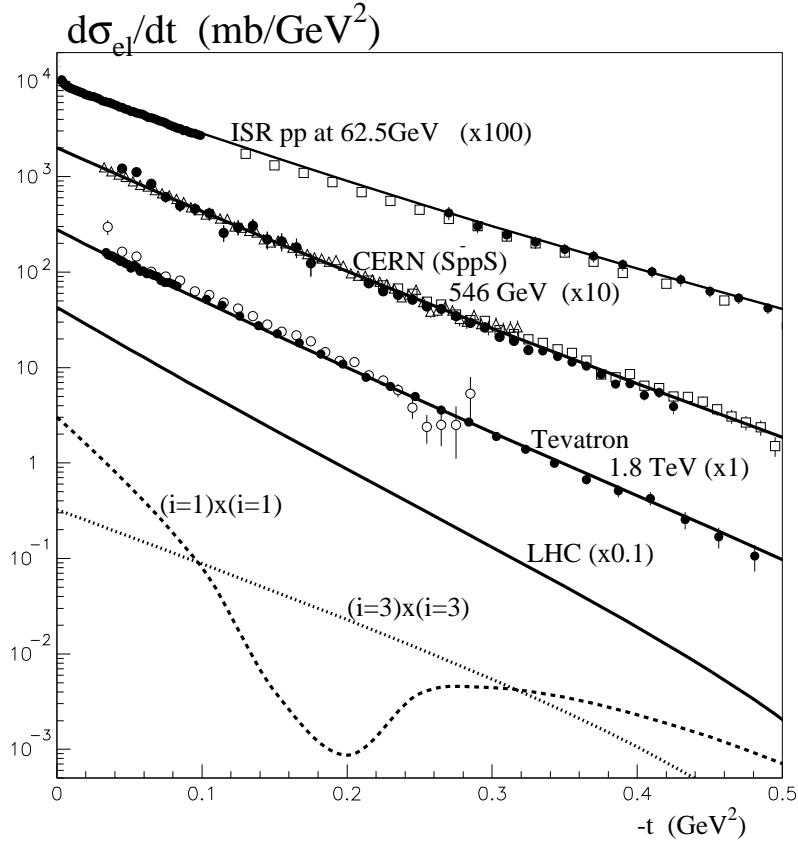


Figure 9: The t dependence of the elastic pp cross section. The dashed and dotted lines are the contributions from the elastic scattering of the largest size ($i = 1$) and the smallest size ($i = 3$) components.

5 Description of the data and predictions for the LHC

Clearly, the number of parameters in our model is too large to perform a straightforward χ^2 fit of the data. Instead, we fix the majority of the parameters at reasonable values and demonstrate that such a model can reproduce all the features of the available data on diffractive cross sections, σ_{tot} , $d\sigma_{el}/dt$, $\sigma_{\text{SD}}^{\text{low}M}$, $d\sigma_{\text{SD}}/dM^2$.

Before we give the values of the parameters, we show in Fig. 9 the quality of the description of the data for the *elastic differential* cross section. We also present in Fig. 9 the prediction for differential elastic cross section at the LHC energy $\sqrt{s} = 14$ TeV. Recall that we are using a three-channel eikonal. That is $i, k = 1, 2, 3$. It is interesting to note that the contribution to the cross section arising from the scattering of the two large-size eigenstates, $(i = 1) \times (i = 1)$, already has a diffractive dip at $-t = 0.2$ GeV^2 . However, after the contributions from all possible combinations $i \times k$ are summed up, the prediction has no dip up to $-t = 0.5$ GeV^2 .

Note, also, that the Pomeron and secondary Reggeon couplings to the proton were taken to have the forms

$$\beta(t) = \beta_0 e^{d_2 t} / (1 - t/d_1)^2, \quad \beta(t) = \beta_R e^{d_R t}. \quad (52)$$

The values of the parameters that we use are

$$d_2 = 0.15 \text{ GeV}^{-2}, \quad d_1 = 1.5 \text{ GeV}^2, \quad d_R = 1 \text{ GeV}^{-2}. \quad (53)$$

The non-zero value of d_2 is simply to provide good convergence and accuracy of the Fourier transform. The parameter d_1 controls the t behaviour of the elastic cross section, while d_R is responsible for the t slope of diffractive dissociation at relatively low $y = -\ln \xi$, where the cross section is dominated by the RRP triple-Reggeon term. The relative size of this contribution, as compared to that due to PPP , was tuned by choosing $v_{PR} = 1.8$ and $r_{RRP} = 3$. In order to describe the data, the couplings were found to be $\beta_0^2 = 33 \text{ mb}$ and $\beta_R^2 = 8 \text{ mb}$. Since we choose a relatively simple t dependence for the Reggeon-proton couplings $\beta(t)$, our model is only reliable over a restricted t interval, $-t \lesssim 0.5 \text{ GeV}^2$. Note that in this domain, the real part of Pomeron exchange, and a possible Odderon exchange contribution, would give only very small effects.

To describe the high energy behavior of the *total* cross section, we take $\Delta^a = 0.3$ for each of the three components of the Pomeron. These Pomeron intercepts are consistent with resummed NLL BFKL, which gives $\omega_0 \sim 0.3$ practically independent of the scale k_t [29]. The slopes of the Pomeron trajectories are driven by the transverse momentum associated with the particular component a . In fact, we have $\alpha' \propto 1/k_t^2$. We find the data require $\alpha'_{P_1} = 0.05 \text{ GeV}^{-2}$ for the large-size Pomeron component, so we put $\alpha'_{P_2} = 0.05/9 \text{ GeV}^{-2}$ for the second component and $\alpha'_{P_3} = 0$ for the smallest-size component. For the secondary Reggeon trajectory we take $\alpha'_R = 0.9 \text{ GeV}^{-2}$, and $\alpha_R(0) = 0.6$. The ‘bare’ value is a bit larger than $\frac{1}{2}$, since the final effective intercept is reduced by the absorptive corrections included in the evolution equation. The description of the total cross section data are shown in Fig. 10(a). The screening corrections arising from the ‘enhanced’ multi-Pomeron diagrams, that is from the high-mass dissociation, slow down the growth of the cross section with energy. Thus, the model predicts a relatively low total cross section at the LHC – $\sigma_{\text{tot}}(\text{LHC}) \simeq 90 \text{ mb}^{11}$.

5.1 Low-mass dissociation

Recall that the couplings of the Good-Walker eigenstates i were specified by $\beta_i(t) = \gamma_i \beta(\gamma_i t)$. The values $\gamma_1 = 1.80$, $\gamma_2 = 0.82$ and $\gamma_3 = 0.38$ were chosen so as to reproduce the *low-mass dissociation* cross section $\sigma_{\text{SD}}^{\text{low}M} = 2 \text{ mb}$ at the CERN-ISR energy¹² [27].

¹¹This value is also predicted by other models of ‘soft’ interactions which include absorptive effects [30, 31].

¹²Although, here, we use a three-channel eikonal model, practically the same results, and the same quality of the description, is obtained using a two-channel eikonal, that is only two eigenstates $|\phi_i\rangle$ (see also the discussion in [22]).

5.2 High-mass dissociation

The value of the parameter λ , which controls the cross section of *high-mass dissociation* in the small ξ (that is, large y) region, was found to be $\lambda = 0.25$. The dependence of the cross section for high-mass dissociation, $\xi d^2\sigma/dtd\xi$, on $\xi = M^2/s$ is compared with the Tevatron CDF data [32, 33] in Fig. 11. Recall that in our model we have not included pion exchange. Since the $\pi\pi P$ term is essential at large ξ , we have included the corresponding contribution using the parameters obtained in [7]. The results without the $\pi\pi P$ term are shown by the dashed lines. We also show in Fig. 11(a) (by the dotted line at small ξ) the prediction for the LHC energy.

Above, we introduced the different types of data mentioning the parameters that they mainly constrain. Of course, in practice, these parameter values are used to describe all the ‘soft’ data simultaneously.

The energy behaviour of the cross sections are shown in Table 1 and Fig. 10. Fig. 10 also shows the energy behaviour of the multiplicities of the secondaries produced by the t -channel Pomeron components of different sizes; we will discuss the multiplicity distributions in some detail in Section 6.

energy	σ_{tot}	σ_{el}	$\sigma_{\text{SD}}^{\text{low}M}$	$\sigma_{\text{SD}}^{\text{high}M}$	$\sigma_{\text{SD}}^{\text{tot}}$
1.8	73.7	16.4	4.1	9.7	13.8
14	91.7	21.5	4.9	14.1	19.0
100	108.0	26.2	5.6	18.6	24.2

Table 1: Cross sections (in mb) versus collider energy (in TeV).

The values of $\sigma_{\text{SD}}^{\text{tot}}$ quoted in Table 1 look, at first sight, too large, when compared with the value 9.46 ± 0.44 mb given by CDF [32]. However the CDF value does not include the secondary Reggeon (RRP) contribution, denoted as a ‘non-diffractive’ component of 2.6 ± 0.4 mb. Moreover, the trigger used to select the diffractive dissociation events rejects part of the low-mass proton excitations. Taking these absences into account, there is no contradiction between the model prediction and the CDF data. Furthermore, note that in the region where the CDF detector efficiency and resolution are good, our model gives an excellent description of the measured data, see Fig. 11.

It is interesting to note, that after tuning the parameters to describe all the available ‘soft’ data, the model satisfies the Finite Energy Sum Rules [34] to good accuracy¹³. Indeed, we can switch off the low-mass dissociation, putting the same couplings for each diffractive eigenstate ($\gamma_1 = \gamma_2 = \gamma_3 = 1$), and replace the low-mass excitations for $\Delta y < 1.5$ by the triple- and multi-Regge contributions¹⁴. Keeping all the other parameters as before, we then obtain $\sigma_{\text{tot}} = 73$ mb

¹³We thank Alan White for discussions.

¹⁴Recall that in the basic model we introduced a threshold $\Delta y = 1.5$; we started the evolution (29), (30) at $y = 1.5$ in order not to generate low-mass dissociation via triple- and multi-Regge contributions and to avoid double counting.

(93 mb) and $\sigma_{\text{SD}}^{\text{tot}}=13.6$ mb (20.1 mb) for the Tevatron (LHC) energies, These values are close to those in Table 1.

In principle, it is straightforward, although computer intensive, to use the model to calculate the cross section for double dissociation, σ_{DD} . We do not show the values here. The values will be similar to those in Table 2 of Ref. [22]; footnote 25 of that paper shows that the values of σ_{DD} are in excellent agreement with the Tevatron data.

5.3 Central exclusive production

The cross sections for the Central Exclusive Diffractive (CED) production at the LHC energy $\sqrt{s} = 14$ TeV are shown in Fig. 12 for those ξ intervals which can be studied by the TOTEM and FP420 detectors. Here we mean the soft CED production of a state with the mass given by $M^2 = \xi_1 \xi_2 s$ separated from the incoming protons by two large rapidity gaps. The calculation is described in Section 4.5. The cross section integrated over the $0.002 < \xi_i < 0.2$ ($0.02 < \xi_i < 0.2$) intervals (for both ξ_1 and ξ_2) is predicted¹⁵ to be 53 (16) μb . The major contribution comes from pure soft interactions. For $\xi < 0.02$, more than 80% of the cross section is due to the large size component of the Pomeron; and more than half for larger values of ξ . Note that, in the CED calculations, we did not include the $\pi\pi P$ contribution. Thus, actually, the expected cross section will be larger for ξ values that are not too small, see Fig. 11.

Note that the resulting CED cross section is about twice larger than that expected from the naive factorization formula

$$\frac{\xi_1 \xi_2 d\sigma_{\text{CED}}}{d\xi_1 d\xi_2} = \frac{1}{\sigma_{\text{tot}}} \frac{\xi_1 d\sigma_{\text{SD}}}{d\xi_1} \frac{\xi_2 d\sigma_{\text{SD}}}{d\xi_2}. \quad (54)$$

This is due to the fact that each single dissociation contains a gap survival factor $S_{ik}^2(b)$ and therefore the r.h.s. of (54) is proportional to $(S^2)^2$ while the l.h.s. contains S^2 once only. On the other hand, for Central Exclusive Production the typical values of the impact parameter b are smaller; so we have a smaller gap survival factor $\langle S^2(b) \rangle$. This partly compensates the additional power of S^2 in the r.h.s. of (54), and as a result the violation of the factorization shown in (54) is not so strong. We will discuss rapidity gap survival in central exclusive production in detail in the following paper [15].

6 Multiparticle inclusive production

As we have a detailed model for high energy soft processes, it would appear to be possible to predict the multiplicity distribution at the LHC. However, although some general features can

¹⁵To speed up the computation we neglect the small non-zero value of α' in the calculation of the amplitude $\Omega^{aa'}$. Then there is no diffusion in impact parameter space and the integral over \mathbf{b}'_2 disappears; since $\mathbf{b}'_2 = \mathbf{b}_2$. However, to correct the final result we smear out the resulting amplitude, which allows for the larger gap survival probability at larger b . In this way we retain reasonable ($\sim 20\%$) accuracy of the computations.

be predicted, it is not so simple to make a quantitative prediction. We address the problem below.

Recall that in the evolution equations for the *amplitude*, given in (29), (30), we include the absorptive factor $\exp(-\Omega/2)$, and not $\exp(-\Omega)$. That is we work with the forward amplitude $\text{Im}T(b) = 1 - e^{-\Omega/2}$, which at each step of the evolution (in rapidity y) includes all possible processes - both elastic and inelastic interactions with cross sections $\sigma_{\text{el}}(b) = (1 - e^{-\Omega/2})^2$ and $\sigma_{\text{inel}}(b) = 1 - e^{-\Omega}$; where $\sigma_{\text{tot}}(b) = 2\text{Im}T(b) = \sigma_{\text{el}}(b) + \sigma_{\text{inel}}(b)$, see eqs. (5)-(7).

As usual, inelastic processes include both single-ladder exchange, as well as multiple interactions with a larger density of secondary partons. The situation is similar to the rescattering of a fast hadron in a heavy nucleus. That is, in such an eikonal approach the probability, $w_N(b)$, of events with parton multiplicity N times larger than that in a single ladder, is given by

$$w_N = \frac{\Omega^N}{N!} e^{-\Omega}. \quad (55)$$

In the multi-channel case the opacity Ω should be replaced by F_{ik} . Unfortunately, we cannot use this probability w_N literally to describe the multiplicity distributions of secondary *hadrons*. In particular a non-negligible fraction of the final hadrons may be produced via the fragmentation of minijets. These processes are beyond the ‘pure soft’ approach used in the present paper. Therefore, below, we discuss the multiplicity distribution only at the partonic level.

The mean number of the (t -channel) ladders of the type a produced in the collision of i and k Good-Walker eigenstates can be calculated as

$$N_{ik}^a(\mathbf{b}) = \frac{1}{\beta_0^2 \sigma_{ik}(\mathbf{b})} \int \Omega_k^a(y, \mathbf{b}_1, \mathbf{b}_2) \Omega_i^a(Y - y, \mathbf{b}_1, \mathbf{b}_2) d^2b_1 d^2b_2 \delta^{(2)}(\mathbf{b}_1 - \mathbf{b}_2 - \mathbf{b}). \quad (56)$$

where $\sigma_{ik}(\mathbf{b}) = 2[1 - \exp(-F_{ik}(\mathbf{b})/2)]$ and $a = P_1, P_2, P_3, R$. Recall that P_1 , P_2 and P_3 are the large, intermediate and small size components of the Pomeron respectively. After averaging over the impact parameter \mathbf{b} and the diffractive eigenstates i, k of the incoming protons, we obtain

$$N_{\text{tube}}^a = \frac{1}{\sigma_{\text{tot}} \beta_0^2} \sum_{i,k} |a_i|^2 |a_k|^2 \int \Omega_k^a(y, \mathbf{b}_1, \mathbf{b}_2) \Omega_i^a(Y - y, \mathbf{b}_1, \mathbf{b}_2) d^2b_1 d^2b_2. \quad (57)$$

This quantity may be considered as the mean number of colour tubes of type a produced in the proton-proton interaction. Note that the value of N_{tube}^a does not depend¹⁶ on the rapidity y .

To obtain the number of partons created by the ladder ‘ a ’ at rapidity y , we have to include the parton density $\rho^a(y)$ of (33) in the numerator of (57). That is

$$N_{\text{parton}}^a = \frac{1}{\sigma_{\text{tot}} \beta_0^2} \sum_{i,k} |a_i|^2 |a_k|^2 \int \Omega_k^a(y, \mathbf{b}_1, \mathbf{b}_2) \rho_{ik}^a \Omega_i^a(Y - y, \mathbf{b}_1, \mathbf{b}_2) d^2b_1 d^2b_2. \quad (58)$$

The results are shown in Fig. 10(d). The main growth in multiplicity, as we go from Tevatron to LHC energies, is due to the small size (‘QCD’) Pomeron component, which produces particles with typically $p_t \sim 5$ GeV. There is essentially no growth in multiplicity at small p_t . This

simply confirms the trend that has been observed through the CERN-ISR to Tevatron energy range, see the data points in Fig. 13.

In other words, starting with the same intercepts ($\Delta = 0.3$) the large size component contribution after the absorptive correction becomes practically flat, while the small size contribution, which is much less affected by the absorption, continues to grow with energy. As mentioned above, such a behaviour is consistent with the experiment (see Fig. 13) where the density of a low k_t secondaries is practically saturated while probability to produce a hadron with a large (say, more than 5 GeV) transverse momentum grows with the initial energy.

Unfortunately we cannot identify each ‘parton’ with a pion. At a large k_t it is probable that, after the hadronisation, a parton forms a gluon jet of pions. However, at low k_t this is not evident; it is hard to say what a gluon ‘jet’ becomes at a low k_t . Nevertheless, in order to compare the model with the data we assume, that after hadronisation, each parton from Pomeron components P_1 , P_2 and P_3 gives three charged pions with $p_{ti} \sim 0.5$, 1.5 and 5 GeV respectively. In this way we may estimate the inclusive cross section, at the three values of p_t , using

$$\frac{Ed\sigma^{ch}}{d^3p} = \frac{3\sigma_{\text{tot}}N_{\text{parton}}^{P_i}}{\pi p_{ti}^2}, \quad (59)$$

where σ_{tot} allows for normalisation and $1/p_t^2$ accounts for the size of the phase space occupied by the particles from component i .

To obtain a qualitative feel for the expected behaviour, we show our predictions at the Tevatron and LHC energies in Fig.13, where the horizontal lines indicate the typical p_t interval associated with each Pomeron component. Recall, that in our ‘soft’ model, we never use the *value* of the Pomeron k_t explicitly. The characteristic parameters actually used in the computations are the *ratios* $k_{t_i}^2/k_{t_{i+1}}^2$. The horizontal lines reflect the p_t intervals covered by the various components arising from the scale choices. Some features of Fig.13 are clear. First, although there is some freedom in assigning the overall scale, nevertheless, it appears that the scale choice made in the figure agrees satisfactorily with the Tevatron data [35]. Second, as compared to the Tevatron, the LHC distribution is more enhanced at large p_t . The enhancement is a factor of 2.6 for the ‘QCD’ small-size component of the Pomeron, whereas it is only 1.25 for the ‘soft’ Pomeron component.

7 Summary

New triple-Regge analyses [7, 36], which include absorptive effects, found that the triple-Pomeron coupling is rather large ($g_{3P} = \lambda g_N$ with $\lambda \gtrsim 0.2$). Thus, in order to obtain reliable predictions for diffractive processes at the LHC, it is necessary to have a model of ‘soft’ high-energy processes which includes multi-Pomeron interactions.

¹⁶This was checked by straightforward computation.

Here we have presented such a model, tuned to the existing ‘soft’ data, which, in principle, is capable of predicting the basic features of high-energy soft pp interactions. The absorption of intermediate partons is described by conventional $\exp(-\lambda\Omega)$ -type factors. This corresponds to a coupling $g_m^n = nm\lambda^{n+m-2}g_N/2$ of the $n \rightarrow m$ Pomeron vertices.

Briefly, the model has multi-components in both the s - and t -channels. The former are based on a three-channel eikonal approach, together with the inclusion of multi-Pomeron diagrams, so that both low- and high-mass diffractive dissociation are well described. Predictions for the LHC are given. A novel feature of the model is the inclusion of different t -channel exchanges, which allows for small-, intermediate- and large-size components of the exchanged Pomeron, each with a *bare* intercept $\Delta \equiv \alpha_P(0) - 1 = 0.3$. For the large-size component, the slope of the trajectory is $\alpha'_P = 0.05 \text{ GeV}^{-2}$. The large-size Pomeron component is heavily screened by the effect of ‘enhanced’ multi-Pomeron diagrams, associated with high-mass dissociation. This leads, among other things, to the effective “saturation” of the low p_t particle density, and to a slow growth of the total cross section. Indeed, the model predicts a relatively low total cross section at the LHC – $\sigma_{\text{tot}}(\text{LHC}) \simeq 90 \text{ mb}$. On the other hand, the small-size component of the Pomeron is weakly screened, leading to an anticipated growth of the particle multiplicity at large p_t ($\sim 5 \text{ GeV}$) at the LHC. Thus the model has the possibility to embody a smooth matching of the perturbative QCD Pomeron to the ‘soft’ Pomeron.

We emphasized that a reliable model of soft interactions is essential in order to predict the rates of diffractive processes at the LHC. In particular, we used the model to calculate the rapidity gap survival factors, including the effects of *both* eikonal and enhanced rescattering. This is the subject of the following paper [15].

Acknowledgements

We thank Aliosha Kaidalov and Risto Orava for useful discussions. MGR thanks the IPPP at the University of Durham for hospitality. The work was supported by grant RFBR 07-02-00023, by the Russian State grant RSGSS-3628.2008.2.

References

- [1] See, for example,
P.D.B. Collins, Regge theory and high energy physics (Cambridge Univ. Press, 1977)
M.M. Block, Phys. Rept. **436**, 71 (2006);
R. Fiore *et al.*, arXiv:0810.2902 [hep-ph].
- [2] V.N. Gribov, Sov. Phys. JETP **26**, 414 (1968).
- [3] V.N. Gribov and A.A. Migdal, Sov. J. Nucl. Phys. **8**, 583 (1969).

- [4] V.N. Gribov and A.A. Migdal, Sov. Phys. JETP **28**, 784 (1969).
- [5] M. G. Ryskin, A. D. Martin and V. A. Khoze, arXiv:hep-ph/0506272.
- [6] V. A. Khoze, A. D. Martin and M. G. Ryskin, arXiv:0810.3324 [hep-ph].
- [7] E.G.S. Luna, V.A. Khoze, A.D. Martin and M.G. Ryskin, Eur. Phys. J. **C59**, 1 (2009).
- [8] V.A. Khoze, A.D. Martin and M.G. Ryskin, Eur. Phys. J. **C55**, 363 (2008).
- [9] V.A. Khoze, A.D. Martin and M.G. Ryskin, Eur. Phys. J. **C23**, 311 (2002).
- [10] V.A. Khoze, A.D. Martin and M.G. Ryskin, Eur. Phys. J. **C14**, 525 (2000).
- [11] A. De Roeck, V.A. Khoze, A.D. Martin, R. Orava and M.G. Ryskin, Eur. Phys. J. C **25**, 391 (2002).
- [12] M. Albrow and A. Rostovtsev, arXiv:hep-ph/0009336;
M. G. Albrow *et al.* [FP420 R and D Collaboration], arXiv:0806.0302 [hep-ex].
- [13] V.A. Khoze, A.D. Martin and M.G. Ryskin, Eur. Phys. J. **C19**, 477 (2001), Erratum **C20**, 599 (2001); arXiv:hep-ph/0006005.
- [14] V.A. Khoze, A.D. Martin and M.G. Ryskin, Eur. Phys. J. **C18**, 167 (2000).
- [15] M.G. Ryskin, A.D. Martin and V.A. Khoze, arXiv:0812.2413 [hep-ph].
- [16] M.L. Good and W.D. Walker, Phys. Rev. **120**, 1857 (1960);
E.L. Feinberg and I.Ya. Pomeranchuk, Doklady Akad. Nauk SSSR **93**, 439 (1953); Suppl. Nuovo Cimento v. **III**, serie X, 652 (1956).
- [17] V.A. Abramovsky, V.N. Gribov and O.V. Kancheli, Sov. J. Nucl. Phys. **18**, 308 (1973).
- [18] R.D. Field and G.C. Fox, Nucl. Phys. **B80**, 367 (1974);
A.B. Kaidalov, V.A. Khoze, Yu.F. Pirogov and N.L. Ter-Isaakyan, Phys. Lett. **B45** 471 (1974);
for a review see A.B. Kaidalov, Phys. rep. **50**, 157 (1979).
- [19] A. Capella, J. Kaplan and J. Tran Thanh Van, Nucl. Phys. B **105**, 333 (1976).
- [20] J. Bartels, M.G. Ryskin and G.P. Vacca, Eur. Phys. J. **C27**, 101 (2003).
- [21] ZEUS collaboration: Abstract 549, Int. Europhysics Conf. on HEP, Aachen, July 2003.
- [22] M.G. Ryskin, A.D. Martin and V.A. Khoze, Eur. Phys. J. **C54**, 199 (2008).
- [23] D. Amati, A. Stanghellini and S. Fubini, Nouvo Cim. **26**, 896 (1962).

- [24] E.L. Feinberg and D.S. Chernavski, Usp. Fiz. Nauk **82**, 41 (1964);
 V.N. Gribov, Sov. J. Nucl. Phys. **9**, 369 (1969);
 V.N. Gribov, in *Gauge Theories and Quark Confinement*, PHASIS, Moscow, 2002, p.3.
- [25] L.N. Lipatov, Sov. Phys. JETP **63**, 904 (1986).
- [26] V.S. Fadin, E.A. Kuraev, and L.N. Lipatov, Phys. Lett. B **60**, 50 (1975);
 E.A. Kuraev, L.N. Lipatov, and V.S. Fadin, Zh. Eksp. Teor. Fiz. **71**, 840 (1976) [Sov. Phys. JETP **44**, 443 (1976)]; *ibid.* **72**, 377 (1977) [**45**, 199 (1977)];
 I.I. Balitsky and L.N. Lipatov, Yad. Fiz. **28**, 1597 (1978) [Sov. J. Nucl. Phys. **28**, 822 (1978)].
- [27] L. Baksay *et al.*, Phys. Lett. **B53** 484 (1975);
 R. Webb *et al.*, Phys. Lett. **B55** 331 (1975);
 L. Baksay *et al.*, Phys. Lett. **B61** 405 (1976);
 H. de Kerret *et al.*, Phys. Lett. **B63** 477 (1976);
 G.C. Mantovani *et al.*, Phys. Lett. **B64** 471 (1976).
- [28] M. Albrow *et al.*, arXiv:0811.0120 [hep-ex].
- [29] V.S. Fadin and L.N. Lipatov, Phys. Lett. **B429**, 127 (1998);
 G. Camici and M. Ciafaloni, Phys. Lett. **B430**, 349 (1998);
 G.P. Salam, JHEP **9807**, 019 (1998), Act. Phys. Pol. **B30**, 3679 (1999);
 M. Ciafaloni, D. Colferai and G.P. Salam, Phys. Lett. **B452**, 372 (1999), Phys. Rev. **D60**, 114036 (1999).
- [30] S. Sapeta and K.J. Golec-Biernat, Phys. Lett. **B613**, 154 (2005).
- [31] E. Gotsman, E. Levin, U. Maor and J.S. Miller, arXiv:0805.2799.
- [32] F. Abe *et al.*, [CDF collaboration] Phys. Rev. **D50** 5535 (1994).
- [33] K. Goulianos and J. Montanha, Phys. Rev. **D59** 114017 (1999).
- [34] R. Dolen, D. Horn and C. Schmid, Phys. Rev. **166**, 1768 (1968).
- [35] CDF Collaboration, F. Abe *et al.*, Phys. Rev. Lett. **61**, 1819 (1988).
- [36] T. Poghosyan and A.B. Kaidalov, private communication.

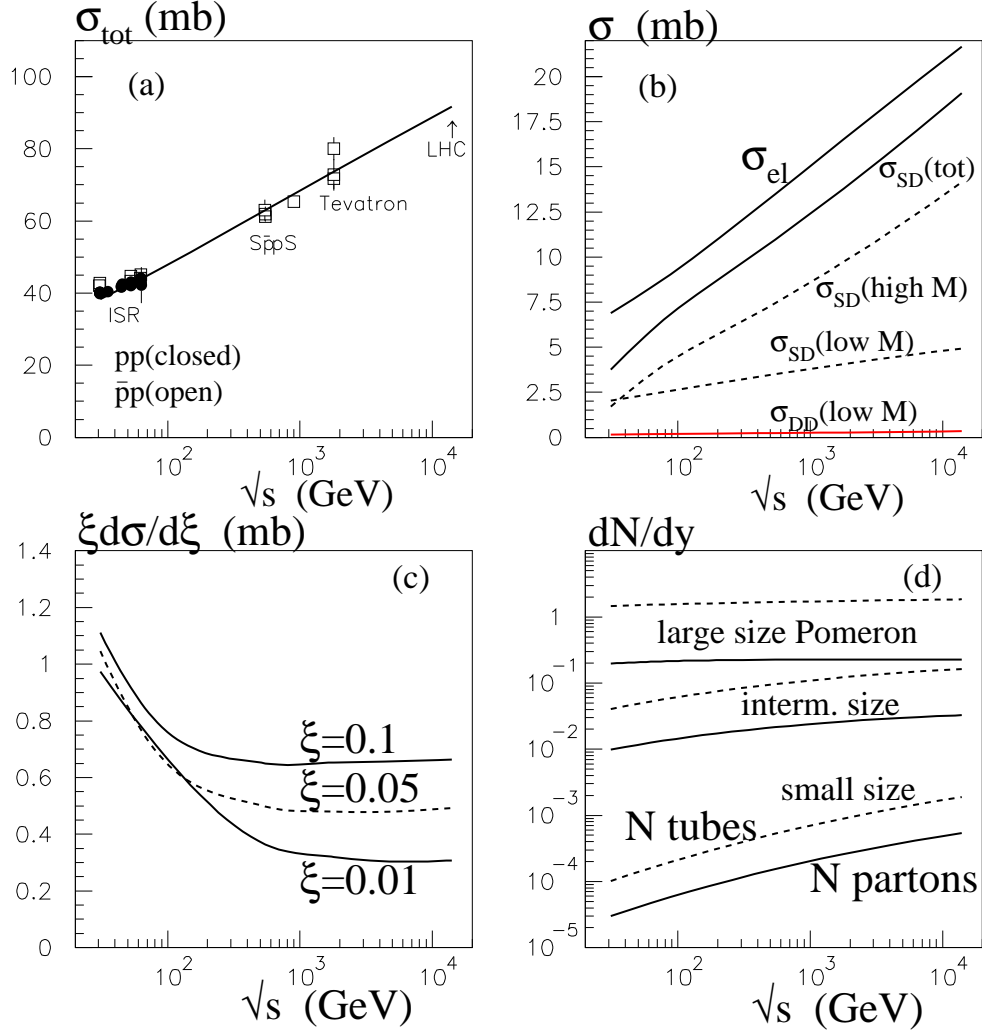


Figure 10: The energy dependence of the total (a), elastic and diffractive dissociation (b) pp cross sections and the cross sections of dissociation to a fixed $M^2 = \xi s$ state (c); (d) the parton multiplicity (solid lines) and the number of 'colour tubes' (dashed) produced by the Pomeron components of different size.

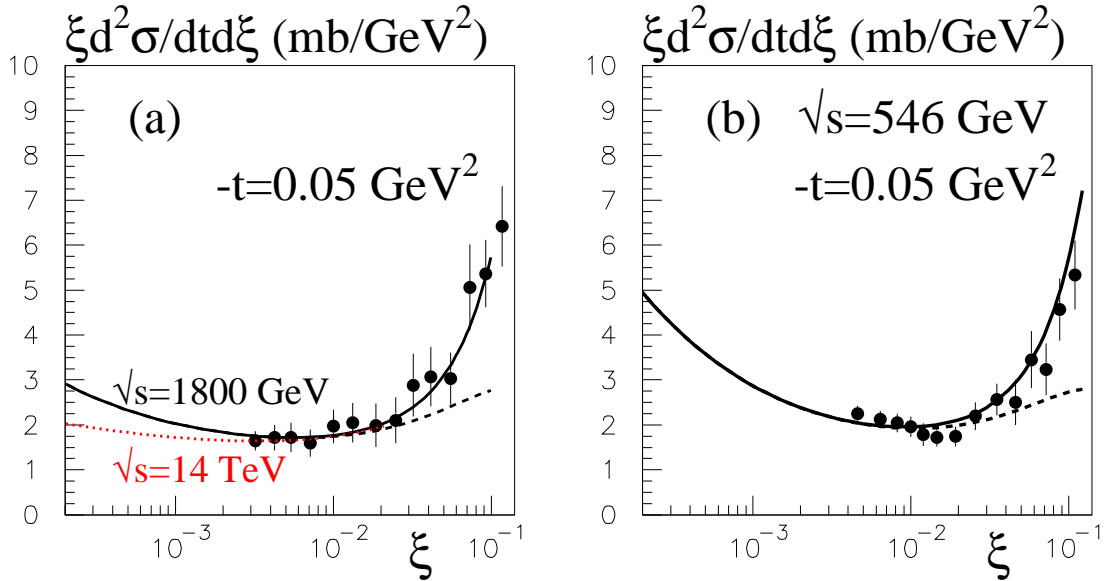


Figure 11: The model description of the data for the cross section for high-mass dissociation versus ξ for $-t = 0.05 \text{ GeV}^2$ at $\sqrt{s} = 1800 \text{ GeV}$ and 546 GeV [32, 33]. The dashed lines are the predictions without the $\pi\pi P$ contribution. The dotted curve at small ξ is the prediction for the LHC.

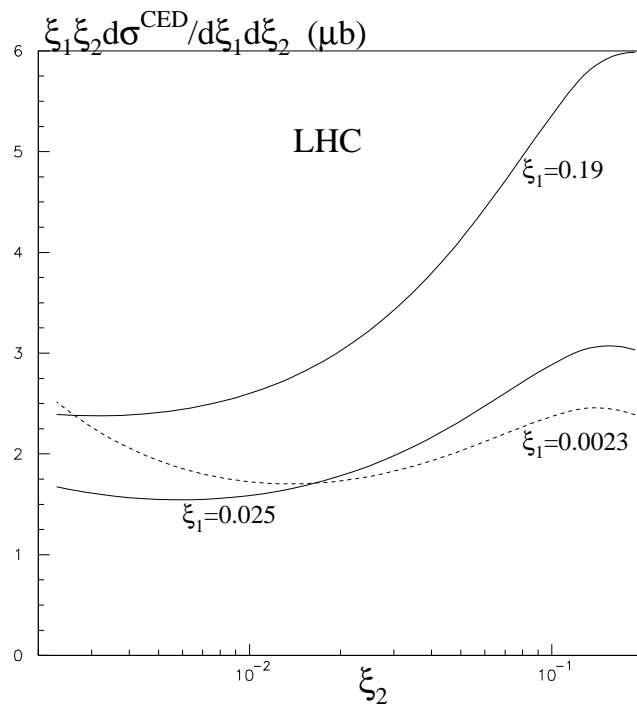


Figure 12: Sample predictions for Central Exclusive Diffractive production at the LHC. The ξ_i 's are the momentum fractions of the incoming protons transferred across the rapidity gaps on either side of the centrally produced system of mass $M = \sqrt{\xi_1 \xi_2 s}$.

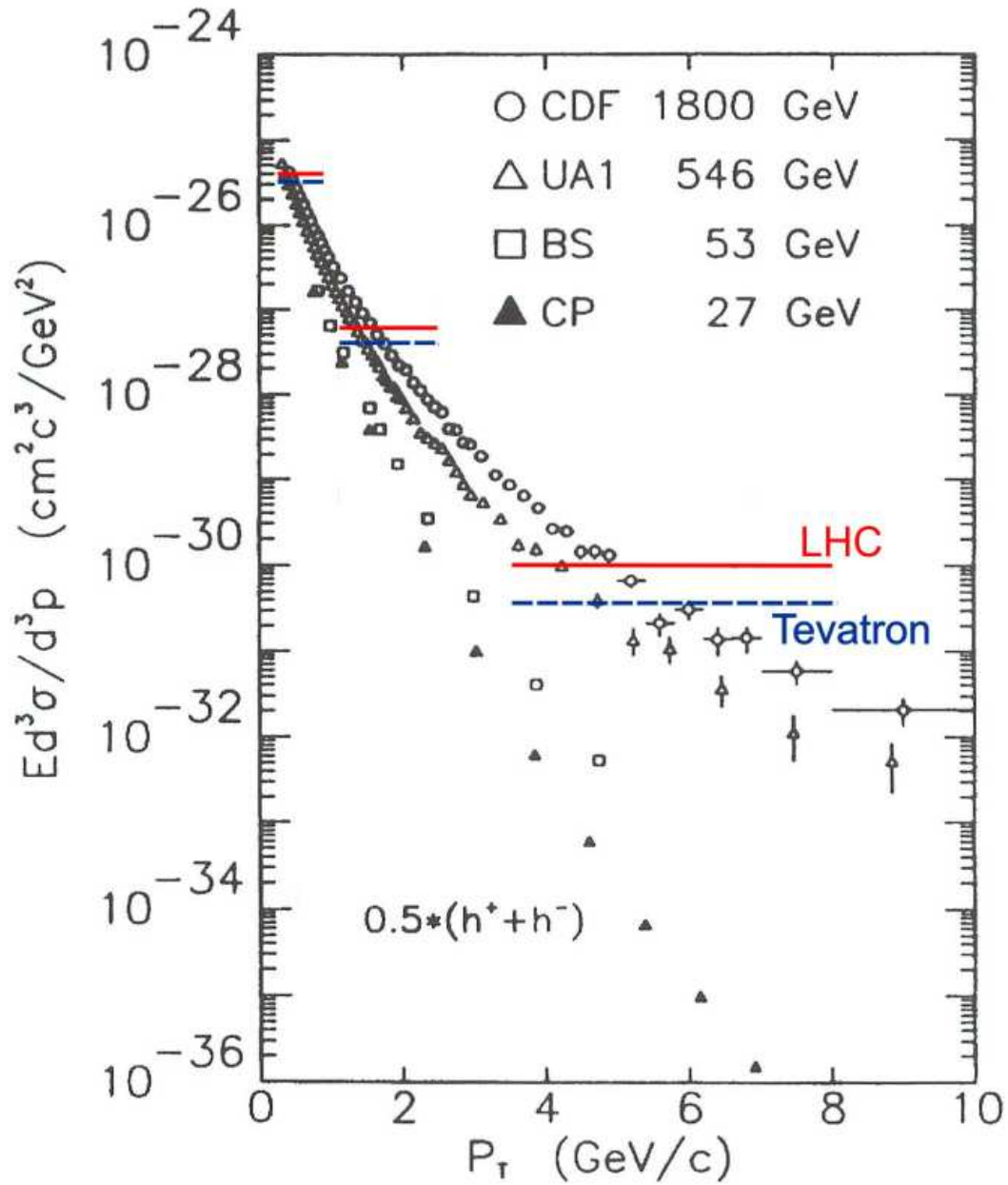


Figure 13: The plot is from Ref. [35]. The horizontal lines, which are superimposed, are our model predictions at the Tevatron and LHC energies; the three p_t ranges correspond to the large-, intermediate- and small-size components of the Pomeron.